



Geophysical Research Letters[®]

RESEARCH LETTER

10.1029/2024GL109481

Key Points:

- Electron trapping dynamics in the formation of quasi-parallel chorus subpackets have been investigated
- The linkage between electron trapping period and subpacket period is quantified via a geometric relation, where the trapping period is shorter
- The proposed relation between electron trapping period and subpacket period is an extension of the classical results of O'Neil (1965)

Supporting Information:

Supporting Information may be found in the online version of this article.

Correspondence to:

H. Chen and X. Wang,
huayue_chen@foxmail.com;
wangxue@auburn.edu

Citation:

Chen, H., Wang, X., Chen, L., Zhang, X.-J., Omura, Y., Chen, R., et al. (2024). Nonlinear electron trapping through cyclotron resonance in the formation of chorus subpackets. *Geophysical Research Letters*, 51, e2024GL109481. <https://doi.org/10.1029/2024GL109481>

Received 26 MAR 2024

Accepted 26 APR 2024

Nonlinear Electron Trapping Through Cyclotron Resonance in the Formation of Chorus Subpackets

Huayue Chen¹ , Xueyi Wang¹ , Lunjin Chen² , Xiao-Jia Zhang² , Yoshiharu Omura³ , Rui Chen¹ , Yi-Kai Hsieh³ , Yu Lin¹ , and Zhiyang Xia²

¹Department of Physics, Auburn University, Auburn, AL, USA, ²William B. Hanson Center for Space Sciences, University of Texas at Dallas, Richardson, TX, USA, ³Research Institute for Sustainable Humanosphere, Kyoto University, Kyoto, Japan

Abstract Chorus subpackets are the wave packets with modulated amplitudes in chorus waves, commonly observed in the magnetospheres of Earth and other planets. Nonlinear wave-particle interactions have been suggested to play an important role in subpacket formation, yet the corresponding electron dynamics remain not fully understood. In this study, we have investigated the electron trapping through cyclotron resonance with subpackets, using a self-consistent general curvilinear plasma simulation code simulation model in dipole fields. The electron trapping period has been quantified separately through electron dynamic analysis and theoretical derivation. Both methods indicate that the electron trapping period is shorter than the subpacket period/duration. We have further established the relation between electron trapping period and subpacket period through statistical analysis using simulation and observational data. Our study demonstrates that the nonlinear electron trapping through cyclotron resonance is the dominant mechanism responsible for subpacket formation.

Plain Language Summary The spectrum of chorus waves comprises a series of subpackets, characterized by modulated amplitudes within a timescale of ~10–100 milliseconds. In this study, we have investigated the self-consistent wave-particle interactions with subpackets, using two-dimensional particle-in-cell simulations in dipole fields. Cyclotron resonant electrons are trapped in wave phases, and we have measured their trapping period. Since these electrons move in the opposite direction of subpacket propagation, the corresponding trapping period is smaller than the period of subpackets. We have further established the relation between the two periods and validated it through both simulation and observational data. This relation facilitates evaluating electron trapping period from direct measurement of subpackets in observations. Our study sheds important lights on the key role of nonlinear electron trapping through cyclotron resonance in the formation of subpackets.

1. Introduction

Chorus subpackets consist of wave packets characterized by modulated amplitudes, typically within a timescale of ~10–100 milliseconds in the Earth's magnetosphere (Goyal et al., 2017; Mourenas et al., 2022; Santolík et al., 2003; Tsurutani et al., 2009; Zhang et al., 2020). They are also observed in the magnetospheres of other planets (Menietti et al., 2012; Reinleitner et al., 1984), as well as in laboratory plasma (Van Compernolle et al., 2016). Subpackets are scientifically interesting due to their significant roles in modulating electron dynamics through nonlinear wave-particle interactions (H. Chen et al., 2022; Crabtree, Ganguli, & Tejero, 2017; Hanzelka et al., 2020; Mourenas et al., 2022; Nogi & Omura, 2022; Nunn et al., 2021; Tao et al., 2017; Zonca et al., 2022). They are believed to cause the fine structures (~10 milliseconds) observed in pulsating auroras (Kataoka et al., 2012; Miyoshi et al., 2015; Ozaki et al., 2018), and contribute to the acceleration of relativistic electrons in the outer radiation belt (Foster et al., 2017; Hiraga & Omura, 2020; Kubota & Omura, 2018).

It is believed that the intense chorus subpackets are generated due to nonlinear electron trapping through cyclotron resonance (H. Chen, Wang, Chen, Omura, Lu, et al., 2023; Chen, Wang, Chen, Omura, Tsurutani, et al., 2023; Demekhov et al., 2020; Hanzelka et al., 2020; Omura, 2021; Tao et al., 2017; Wang et al., 2024). Previous literature speculated that the energy transfer process during subpacket formation is similar to that in Landau resonance, where the energy transfer between subpackets and resonant electrons is conserved (Tao et al., 2017). A necessary condition in this process is the trapping period of resonant electrons being comparable to the subpacket period/duration (O'Neil, 1965). However, Wang et al. (2024) found in simulations that the energy transfer between resonant electrons and subpackets reaches the maximum at the peak amplitudes of subpackets. Moreover,

© 2024. The Authors.

This is an open access article under the terms of the Creative Commons Attribution-NonCommercial-NoDerivs License, which permits use and distribution in any medium, provided the original work is properly cited, the use is non-commercial and no modifications or adaptations are made.

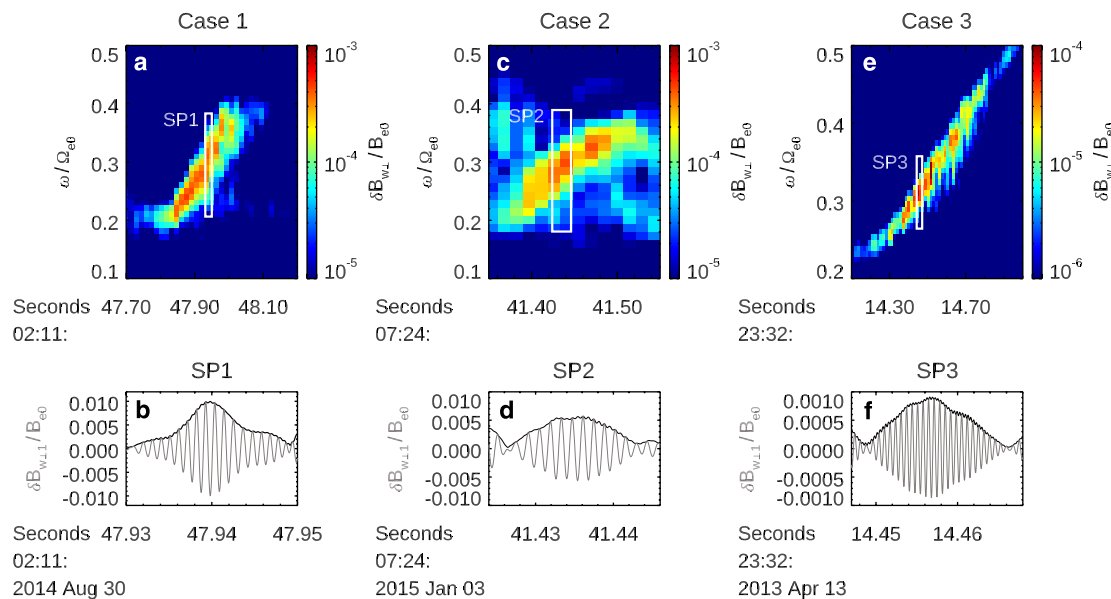


Figure 1. (a, c, e) Spectra of perpendicular magnetic amplitude $\delta B_{w\perp}$ for three chorus wave cases observed by Van Allen Probes. Three subpackets (SP1–SP3) are highlighted by white boxes. (b, d, f) Temporal evolutions of $\delta B_{w\perp}$ (black) and the $\delta B_{w\perp1}$ component (gray) of the three subpackets.

Crabtree, Tejero, et al. (2017) estimated the electron trapping period in one observational event, showing that it is smaller than the subpacket period. Therefore, the mechanism responsible for subpacket formation and the associated electron trapping dynamics remain not fully understood. Note that we concentrate on intense subpackets. There are also moderately intense and very short subpackets in observations, which are proposed to be generated due to wave superposition (Mourenas et al., 2022; Nunn et al., 2021; Zhang et al., 2020).

In this study, we quantify the electron trapping period in the formation of quasi-parallel subpackets, using both satellite observations and self-consistent simulations. Our results indicate that the electron trapping period is smaller than the subpacket period. We further demonstrate that the nonlinear wave-particle interaction through cyclotron resonance is the mechanism responsible for subpacket formation.

2. Satellite Observations

2.1. Observational Cases

We first evaluate the period of subpackets in observations. Three rising tone chorus cases detected by Van Allen Probes in previous literature are selected: Case 1 from R. Chen et al. (2022), Case 2 from Zhang et al. (2018), and Case 3 from Tsurutani et al. (2020). Figures 1a, 1c, and 1e show the spectra of perpendicular magnetic amplitude $\delta B_{w\perp}$ for chorus waves. Within these spectra, three subpackets (SP1, SP2, and SP3) marked by white boxes are chosen. Temporal evolutions of wave magnetic amplitude $\delta B_{w\perp}$ (black) and the $\delta B_{w\perp1}$ component (gray) in these subpackets are shown in Figures 1b, 1d, and 1f. The reverse period of each subpacket ω_{subp} is estimated by identifying the adjacent minimum values of $\delta B_{w\perp}$, and is $\omega_{subp}/\Omega_{e0} = 0.017, 0.021$, and 0.012 for the subpackets SP1–SP3. Here, $\Omega_{e0} = B_{e0}e/m_e$ is the equatorial electron gyrofrequency, e and m_e are the charge and mass of an electron, and B_{e0} is the equatorial background magnetic field.

2.2. Modified Electron Trapping Frequency From Nonlinear Theory

Nonlinear theory indicates that the motion of cyclotron resonant electrons in wave phases can be described by (Nunn, 1986; Omura et al., 2008; Tao et al., 2017)

$$\frac{d^2\zeta}{dt^2} = \omega_{tr_NL}^2|_{S=0}(\sin \zeta + S), \quad (1)$$

where ζ represents the gyrophase angle between electron perpendicular velocity v_{\perp} and wave perpendicular magnetic field $\delta B_{w\perp}$, and S is the inhomogeneity factor. Here, $\omega_{tr-NL}|_{S=0}$ is the trapping frequency of electrons near the stable equilibrium point at $\zeta_0 = \pi$ with $S = 0$, given by

$$\omega_{tr-NL}|_{S=0} = \chi \sqrt{ek_{\parallel}v_{\perp}\delta B_{w\perp}/(m_e\gamma)}, \quad (2)$$

where $\chi = \sqrt{1 - \omega^2/(k^2c^2)}$ with the light speed c , k_{\parallel} is the parallel wave number, and $\gamma = 1/\sqrt{1 - v^2/c^2}$ is the relativistic factor. The stable equilibrium point ζ_0 and the inhomogeneity factor S satisfy

$$\sin \zeta_0 = -S, \quad (3)$$

and

$$|S| < 1, \quad (4)$$

respectively. We expand Equation 1 near ζ_0 as

$$\frac{d^2\zeta}{dt^2} \simeq \omega_{tr-NL}|_{S=0} [\sin \zeta_0 + S + \cos \zeta_0(\zeta - \zeta_0)]. \quad (5)$$

Considering Equation 3, we have

$$\frac{d^2(\zeta - \zeta_0)}{dt^2} \simeq \omega_{tr-NL}|_{S=0} \cos \zeta_0(\zeta - \zeta_0), \quad (6)$$

with $\cos \zeta_0 < 0$. Using S to replace ζ_0 , Equation 6 becomes

$$\frac{d^2(\zeta - \zeta_0)}{dt^2} \simeq -\omega_{tr-NL}|_{S=0} \sqrt{1 - S^2}(\zeta - \zeta_0), \quad (7)$$

or

$$\frac{d^2(\zeta - \zeta_0)}{dt^2} \simeq -\omega_{tr-NL}^2(\zeta - \zeta_0). \quad (8)$$

Here, ω_{tr-NL} represents the modified electron trapping frequency corresponding to a specific ζ_0 , and is given as

$$\omega_{tr-NL} = \omega_{tr-NL}|_{S=0}(1 - S^2)^{1/4} = \chi \sqrt{ek_{\parallel}v_{\perp}\delta B_{w\perp}/(m_e\gamma)}(1 - S^2)^{1/4} \quad (9)$$

The wave frequencies of the three subpackets in observations are $\omega/\Omega_{e0} = 0.28, 0.29$, and 0.31 , and the wave normal angles are $\theta = 9.52^\circ, 25.17^\circ$, and 20.60° , respectively. Based on cold plasma dispersion relation, the wave numbers are estimated as $kV_{Ae0}/\Omega_{e0} = 0.64, 0.68$, and 0.73 (where $V_{Ae0} = B_{e0}/\sqrt{\mu_0 n_{e0} m_e}$ is the electron Alfvén speed, μ_0 is the vacuum permeability, and n_{e0} is the equatorial plasma density). The average wave amplitudes of subpackets are $\delta B_{w\perp}/B_{e0} = 0.0039, 0.0033$, and 0.0006 , and the S values are $S = -0.32, -0.45$, and -0.35 , respectively. The v_{\perp}/V_{Ae0} is 2.5 (Zhang et al., 2018). Other wave parameters can be found in Table S1 of the Supporting Information S1. The $\omega_{tr-NL}/\Omega_{e0}$ in the three subpackets are $0.067, 0.062$, and 0.030 , respectively. These values are $2.5\text{--}4$ times larger than $\omega_{subp}/\Omega_{e0}$ ($=0.017, 0.021$, and 0.012 , respectively), which is consistent with the results in Crabtree, Tejero, et al. (2017).

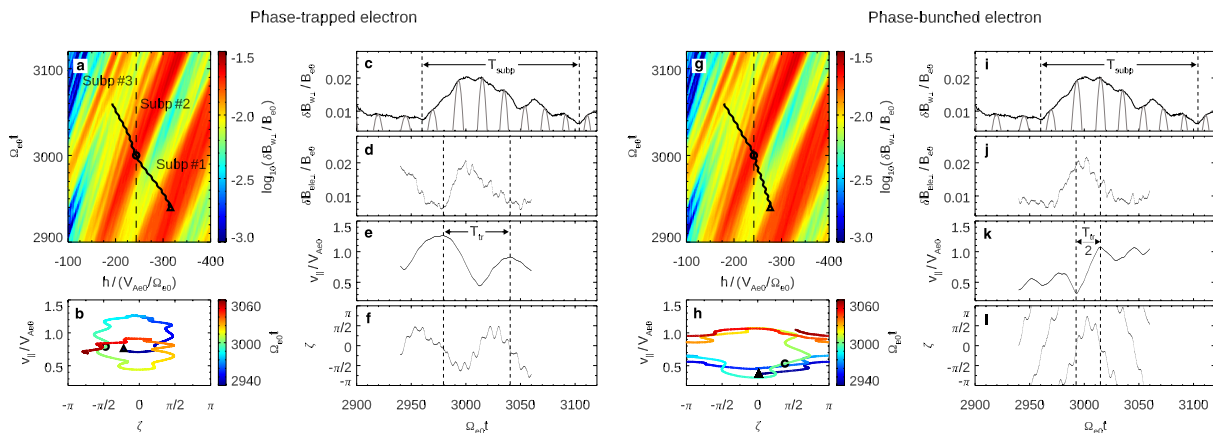


Figure 2. Trajectories of two cyclotron resonant electrons in the (a), (g) $h - t$ planes and (b), (h) $\zeta - v_{\parallel}$ planes, with triangles (circles) indicating the positions at $\Omega_{e0}t = 2,940 (=3,000)$. The left (right) panels depict the trajectories of a phase-trapped (phase-bunched) electron. In panels (a), (g), dashed lines denote the positions of $h/(V_{Aeo}/\Omega_{e0}) = -242.24$, and the color codes in panels (b), (h) represent temporal evolution. In panel (a), three subpackets are labeled as Subp #1–#3. (c), (i) Temporal evolutions of wave magnetic amplitude $\delta B_{w\perp}$ (black) and the $\delta B_{w\perp 1}$ component (gray) at $h/(V_{Aeo}/\Omega_{e0}) = -242.24$. Temporal evolutions of (d), (j) the magnetic amplitude felt by electrons $\delta B_{ele\perp}$ (e), (k) parallel velocity v_{\parallel} , and (f), (l) gyrophase angle ζ of electrons along their motion trajectories. The dotted lines in panels (c), (i) indicate the period T_{subp} of Subp #2. The dashed lines in panels (d)–(f) represent the trapping period T_{tr} for the phase-trapped electron, and those in panels (j)–(l) represent $T_{tr}/2$ for the phase-bunched electron.

3. Electron Trapping in Self-Consistent Simulations

3.1. Simulation Model

To quantify the relation between electron trapping period and subpacket period, we investigate electron dynamics in the self-consistently excited subpackets. The two-dimensional general curvilinear plasma simulation code (GCPIC) model in dipole fields has been used (Lu et al., 2019; Wang et al., 2024). The initial setup is the same as that in Wang et al. (2024). Specifically, the simulation domain spans a radial distance of $p/(V_{Aeo}/\Omega_{e0}) = 1,511$ –1,767 (with p representing the equatorial distance to the center of the Earth), and in a magnetic latitude range of $\lambda = -31^\circ$ – 31° . The ratio of plasma frequency $\omega_{pe} = \sqrt{n_{e0}e^2/m_e\epsilon_0}$ (where ϵ_0 is the vacuum permittivity) to electron gyrofrequency Ω_{e0} at the center of simulation domain is $\omega_{pe}/\Omega_{e0} = 4.98$. The electrons are pushed by relativistic Lorentz force. In this study, we use the retracing method to analyze the electron dynamics. The resonant electrons are collected at a specific time point T_s , and their velocities and positions are recorded from a time point prior to T_s . Note that these electrons are not treated as test particles, but self-consistently interact with waves.

We focus on the cyclotron resonant electrons interacting with the subpackets at a radial distance of $p/(V_{Aeo}/\Omega_{e0}) = 1,722$ and a magnetic latitude of $\lambda = -7.57^\circ$. The subpackets propagate quasi-parallel to field lines with a wave vector $\mathbf{k} \cdot \mathbf{B}_{e0} < 0$, and their evolution is depicted in Figure 1 of Wang et al. (2024). At $\Omega_{e0}T_s = 3,000$, the wave frequency is $\omega/\Omega_{e0} = 0.33$ and the wave normal angle is $\theta = 16.44^\circ$, leading to the cyclotron resonance velocity of $v_c/V_{Aeo} = 0.76$ ($v_c = (\omega - \Omega_0/\gamma)/k_{\parallel}$, where Ω_0 is the local electron gyrofrequency). Resonant electrons are collected in the ranges of $v_{\parallel}/V_{Aeo} = 0.46$ – 1.06 , $v_{\perp}/V_{Aeo} = 2.0$ – 4.0 , and $\zeta = -\pi$ – $\pi/2$, and their dynamics are investigated in the period $\Omega_{e0}t = 2,940$ – $3,060$.

Cyclotron resonant electrons trapped in wave phases can be categorized into phase-trapped and phase-bunch electrons (Albert et al., 2021; Bortnik et al., 2008; Nunn, 1974; Omura et al., 2008). Phase-trapped electrons remain trapped for several periods, while phase-bunched electrons are only trapped for less than one period. In this study, we identify a total of 2,596 resonant electrons, comprising 1,153 phase-trapped electrons and the remaining 1,443 phase-bunched electrons.

3.2. Typical Examples

The trajectories of a phase-trapped electron and a phase-bunched electron in the (a, g) $h - t$ planes and (b, h) $\zeta - v_{\parallel}$ planes are shown in Figure 2. Here, h represents the distance along a field line to the magnetic equator, with negative values indicating the southern hemisphere. Electron positions at $\Omega_{e0}t = 2,940$ are indicated,

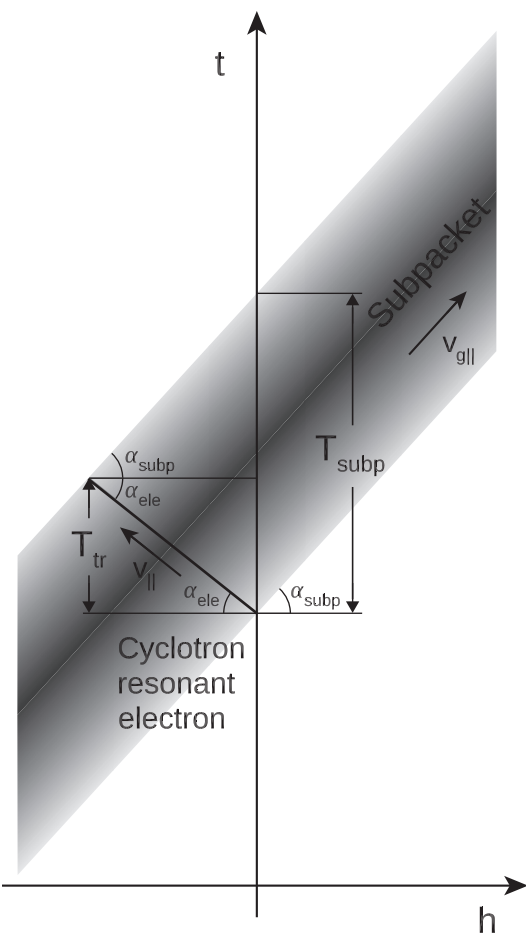


Figure 3. A schematic diagram depicting the propagation of a subpacket and the trajectory of a cyclotron resonant electron in the $h - t$ plane, with the subpacket period denoted by T_{subp} and the electron trapping period denoted by T_{tr} . The subpacket propagates with the parallel group velocity $v_{g\parallel}$, and the electron moves with the parallel velocity $v_{\parallel} \sim v_c$. The two velocities are in opposite directions. The angle between $v_{g\parallel}$ (v_{\parallel}) and the h axis is represented by α_{subp} (α_{ele}).

A schematic diagram comparing T_{tr} and T_{subp} is illustrated in Figure 3, depicting the evolution of a subpacket and the electron trajectory in the $h - t$ plane. The subpacket propagates with a parallel group velocity $v_{g\parallel}$, and the angle between subpacket propagation and the h axis is denoted by $\alpha_{subp} = \tan^{-1}(1/v_{g\parallel})$. The parallel velocity v_{\parallel} of the electron is opposite to $v_{g\parallel}$, and the angle between the electron trajectory and the h axis is determined by $\alpha_{ele} = \tan^{-1}(-1/v_{\parallel})$. For cyclotron resonant electrons, $v_{\parallel} \sim v_c$. The period of a subpacket at a specific position is represented by T_{subp} , and that for resonant electron interacting with waves is T_{tr} . Based on geometric relations, T_{subp} and T_{tr} satisfy

$$T_{subp} = T_{tr} + \frac{T_{tr}}{\tan \alpha_{ele}} \tan \alpha_{subp} = (1 - v_{\parallel}/v_{g\parallel}) T_{tr}. \quad (10)$$

Converting periods to frequencies yields:

$$\omega_{tr} = (1 - v_{\parallel}/v_{g\parallel}) \omega_{subp} \quad (11)$$

and those at $\Omega_{e0}T_s = 3,000$ are denoted by circles. The wave magnetic amplitude $\delta B_{w\perp}$ is overplotted for reference and it contains three subpackets labeled as Subp #1–#3. The subpackets propagate with a negative parallel group velocity $v_{g\parallel}$, while electrons move with a positive parallel velocity v_{\parallel} . During $\Omega_{e0}t = 2,940$ –3,060, the electrons pass through Subp #2. For the phase-trapped electron, the overall trend of v_{\parallel} decreases, and its ζ is confined between $-\pi/2$ and $\pi/2$, indicating continuous trapping in wave phases. While the v_{\parallel} of the phase-bunched electron increases. The electron is only trapped in the wave phases during $\Omega_{e0}t \approx 2,992$ –3,015, with $\zeta \sim \pi/2$.

The subpacket period, which represents the timescale of wave amplitude modulation at a fixed position (Mourenas et al., 2022; Santolík et al., 2003; Tsurutani et al., 2009; Zhang et al., 2020), is then evaluated. At $\Omega_{e0}T_s = 3,000$, the central position of Subp #2 is located at $h/(V_{Aeo}/\Omega_{e0}) = -242.24$. We plot the temporal evolutions of wave magnetic amplitude $\delta B_{w\perp}$ (black) and the $\delta B_{w\perp 1}$ component (gray) at $h/(V_{Aeo}/\Omega_{e0}) = -242.24$ in Figures 2c and 2i. By identifying the adjacent local minimum values of $\delta B_{w\perp}$ at $\Omega_{e0}t = 2,960.0$ and 3,103.4, the period of Subp #2 is estimated as $\Omega_{e0}T_{subp} = 143.4$, and the corresponding reversal is $\omega_{subp} = 2\pi/T_{subp} = 0.044\Omega_{e0}$.

The evolution of wave amplitude at a fixed position differs from that along the electron motion trajectory. Figure 2 shows the temporal evolutions of (d, j) the magnetic amplitude $\delta B_{ele\perp}$ felt by electrons (e, k) parallel velocity v_{\parallel} , and (f, l) gyrophase angle ζ of electrons along their motion trajectories. As v_{\parallel} decreases, ζ tends toward $\sim -\pi/2$; while as v_{\parallel} increases, ζ approaches $\sim \pi/2$. We further quantify the electron trapping period, which represents the timescale of electron interacting with waves during the transversal of a subpacket. Using the adjacent local maximum values of v_{\parallel} around T_s at $\Omega_{e0}t = 2,978.7$ and 3,041.1 (Figure 2d), the trapping period for the phase-trapped electron is measured as $\Omega_{e0}T_{tr} = 62.4$, and the corresponding trapping frequency is $\omega_{tr} = 2\pi/T_{tr} = 0.10\Omega_{e0}$. This period is comparable to the period of $\delta B_{ele\perp}$, indicating that the electron experiences a complete trapping during the transversal. While the phase-bunched electron is only trapped during $\Omega_{e0}t = 2,992.3$ –3,014.4 (Figure 2j), characterized by increasing v_{\parallel} and $\zeta \sim \pi/2$. The electron is trapped for half a period $T_{tr}/2$ during the transversal, with $\Omega_{e0}T_{tr} = 44.2$ and the trapping frequency $\omega_{tr}/\Omega_{e0} = 0.14$. The trapping periods for both types of resonant electrons are smaller than the subpacket period, consistent with observational results (Figure 1).

Equation 11, similar to Equation 27 in Tao et al. (2021), is verified through electron dynamics in Figure 2. During $\Omega_{e0}t = 2,940\text{--}3,060$, the average wave frequency is $\omega/\Omega_{e0} = 0.33$, and the average wave normal angle is $\theta = 15.14^\circ$. Using the cold plasma dispersion relation, the parallel wave number is estimated as $k_{\parallel}V_{Ae0}/\Omega_{e0} = -0.68$, and the parallel group velocity is $v_{g\parallel}/V_{Ae0} = -0.59$. Considering the average parallel velocity of $v_{\parallel}/V_{Ae0} = 0.83 (=0.70)$, the $(1 - v_{\parallel}/v_{g\parallel}) (\omega_{subp}/\Omega_{e0})$ is evaluated as 0.10 (0.09) for the phase-trapped (phase-bunched) electron, and is comparable to the corresponding ω_{tr} . This relation has also been confirmed by electron trapping dynamics simulated in the real-size Earth's magnetosphere, as depicted in Figure S1 of the Supporting Information S1.

By analyzing electron dynamics in simulation, we have quantified that the trapping frequency ω_{tr} is larger than ω_{subp} . We further compare the trapping frequency given by nonlinear theory ω_{tr_NL} with ω_{subp} . For the phase-trapped (phase-bunched) electron, the average magnetic amplitude in the trapping period is $\delta B_{ele\perp}/B_{e0} = 0.014 (=0.012)$, and the average perpendicular velocity is $v_{\perp}/V_{Ae0} = 2.32 (=2.77)$. The inhomogeneity factor is $S = -0.34$ (Wang et al., 2024). Substituting these values and $k_{\parallel}V_{Ae0}/\Omega_{e0} = -0.68$ into Equation 9, we obtain $\omega_{tr_NL}/\Omega_{e0} = 0.14$ for both types of resonant electrons, which is also several times larger than $\omega_{subp}/\Omega_{e0} = 0.044$.

The trapping frequency ω_{tr} is measured in the stationary coordinates through the analysis of electron dynamics. While ω_{tr_NL} is quantified in the reference frame of waves (Denavit & Sudan, 1975; Sudan & Ott, 1971), specifically, in the coordinates moving with the parallel group velocity $v_{g\parallel}$ (Omura et al., 2008). Therefore, there is a Doppler frequency shift between ω_{tr} and ω_{tr_NL} . The two frequencies satisfy

$$\omega_{tr} + k_{subp\parallel}v_{g\parallel} = \omega_{tr_NL}, \quad (12)$$

where $k_{subp\parallel}$ is the reverse spatial scale of a subpacket. The term $k_{subp\parallel}v_{g\parallel}$ is approximately equal to ω_{subp} . Equation 12 can be written as

$$\omega_{tr} + \omega_{subp} \simeq \omega_{tr_NL}. \quad (13)$$

Substituting Equation 11 into Equation 13, we have

$$(2 - v_{\parallel}/v_{g\parallel})\omega_{subp} \simeq \omega_{tr_NL}. \quad (14)$$

Equation 14 presents the relation between the trapping frequency given by nonlinear theory and the reverse period of subpackets.

3.3. Statistical Results

To validate Equation 14, we calculate the theoretical trapping frequency ω_{tr_NL} for each resonant electron using its average v_{\perp} and $\delta B_{ele\perp}$ in the trapping period, and compare it with ω_{subp} . Figure 4 presents the occurrence rates for phase-trapped (red) and phase-bunched electrons (blue) as a function of (a, c) $\omega_{tr_NL}/\omega_{subp}$ and (b, d) $(\omega_{tr_NL}/\omega_{subp})/(2 - v_{\parallel}/v_{g\parallel})$. The occurrence rate is defined as the ratio between the number of phase-trapped (phase-bunched) electrons in each category and the total number of corresponding electrons. For both types of resonant electrons, $\omega_{tr_NL}/\omega_{subp}$ covers a wide range from ~ 2.4 to ~ 4.2 , with the maximum occurrence rate at $\omega_{tr_NL}/\omega_{subp} \sim 3.2$. The values of $\omega_{tr_NL}/\omega_{subp}$ for the three subpackets in observations (SP1-SP3) are also marked at $\omega_{tr_NL}/\omega_{subp} = 4.2, 3.1$, and 2.6 . Therefore, ω_{tr_NL} is several times larger than ω_{subp} . We then quantify the term $2 - v_{\parallel}/v_{g\parallel}$ in simulation and observational data. For each resonant electron in simulation, the average v_{\parallel} and $v_{g\parallel}$ in the trapping period are used. For subpackets SP1-SP3, v_{\parallel} is set as v_c , and $v_{g\parallel}$ is estimated from dispersion relation of chorus waves. After dividing $2 - v_{\parallel}/v_{g\parallel}$, the $(\omega_{tr_NL}/\omega_{subp})/(2 - v_{\parallel}/v_{g\parallel})$ in both simulation and a few selected observational cases are excellently clustered around 1, confirming the relation between ω_{tr_NL} and ω_{subp} in Equation 14.

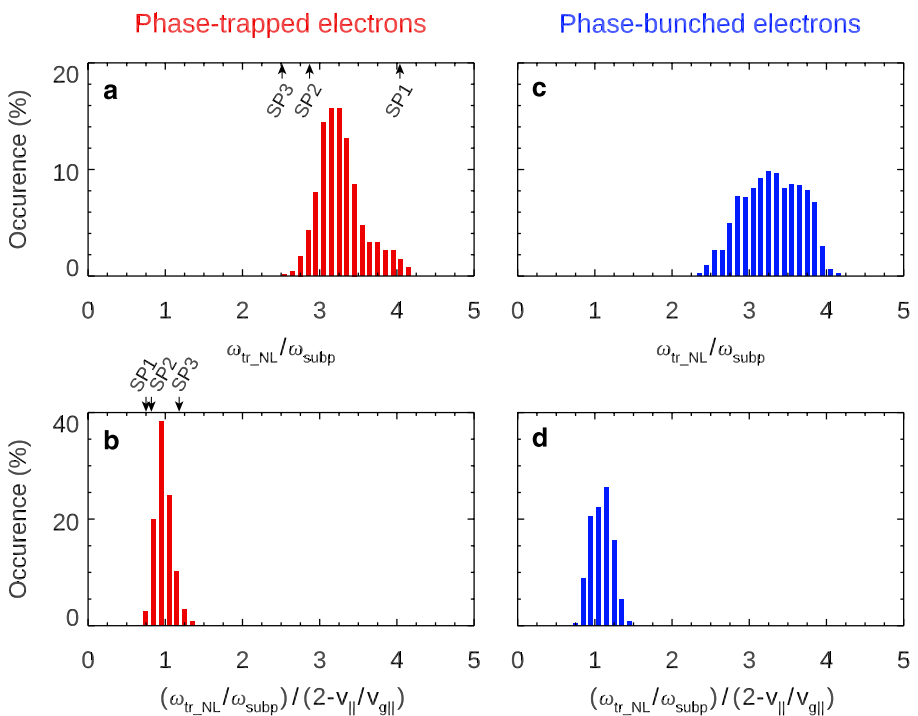


Figure 4. Distributions of occurrence rates for phase-trapped (red) and phase-bunched electrons (blue) as a function of (a), (c) $\omega_{tr_NL}/\omega_{subp}$ and (b), (d) $(\omega_{tr_NL}/\omega_{subp})/(2-v_{||}/v_{g||})$. In panels (a), (b), the values of observational cases SP1-SP3 are indicated by arrows.

4. Summary and Discussion

Using self-consistent GCPIC simulations in dipole fields, we have investigated the nonlinear trapping of cyclotron resonant electrons during chorus subpacket formation. The trapping period has been quantified separately by analyzing electron dynamics and through theoretical derivation, and both methods yield a trapping period smaller than the subpacket period. We have further established the relation between the two periods, and validated it through statistical analysis using simulation and observation data. Our results demonstrate that the nonlinear wave-particle interaction through cyclotron resonance is the dominant mechanism in the formation of quasi-parallel subpackets.

Nonlinear wave-particle interactions have been suggested to play an important role in amplitude modulation of chorus subpackets (H. Chen, Wang, Chen, Omura, Lu, et al., 2023; Chen, Wang, Chen, Omura, Tsurutani, et al., 2023; Crabtree, Ganguli, & Tejero, 2017; Hanzelka et al., 2020; Tao et al., 2017; Zonca et al., 2022). A majority consensus is that the energy transfer between subpackets and particles is conserved (O’Neil, 1965; Tao et al., 2017), similar to the process of Landau resonance in classical models. Landau resonant particles move together with subpackets, and their trapping period is comparable to the subpacket period. The amplitude of subpackets increases (decreases) due to the energy loss (gain) of particles. However, cyclotron resonant particles move in the opposite direction of subpackets, thus their interactions are highly dynamical. The trapping period of cyclotron resonant particles is smaller than the subpacket period (Figure 3). At any specific position, the energy transfer between subpackets and cyclotron resonant particles is not conserved, which will be shown in Figure 5. The amplitude modulation of subpackets at a specific position is determined by both the absolute nonlinear growth rate and the convection term of wave amplitudes (Wang et al., 2024).

We further evaluate the energy transfer between subpackets and particles through Landau resonance ΔW_L and cyclotron resonance ΔW_c in simulation, which are defined as

$$\Delta W_L = - \int_0^\infty \int_0^{2\pi} \int_{-\infty}^0 f(u_{||}, \zeta, u_\perp) ev \cdot \delta Eu_\perp du_{||} d\zeta du_\perp, \quad (15)$$

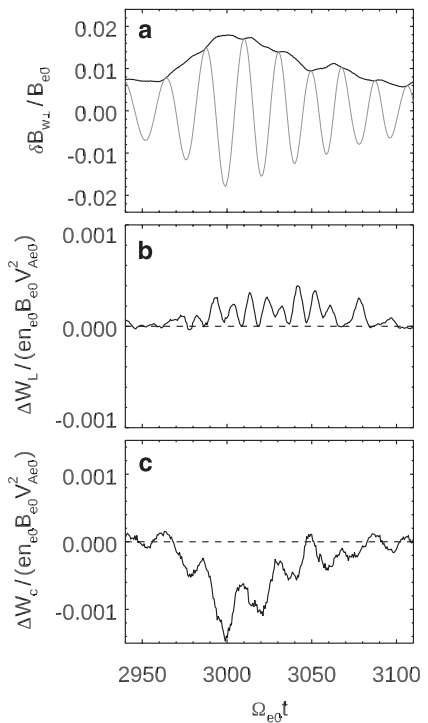


Figure 5. Temporal evolutions of (a) wave magnetic amplitude $\delta B_{w\perp}$ for Subp #2, and the energy transfer through (b) Landau resonance ΔW_L and (c) cyclotron resonance ΔW_c . The dotted lines in panels (b) and (c) denote $\Delta W_L = 0$ or $\Delta W_c = 0$.

and

$$\Delta W_c = - \int_0^\infty \int_0^{2\pi} \int_0^\infty f(u_\parallel, \zeta, u_\perp) ev \cdot \delta Eu_\perp du_\parallel d\zeta du_\perp, \quad (16)$$

where $u = \gamma v$ is the momentum, and $f(u_\parallel, \zeta, u_\perp)$ is the momentum distribution of energetic electrons. A negative (positive) ΔW represents the energy transfer from particles to waves (from waves to particles). Figure 5 shows the temporal evolutions of wave magnetic amplitude $\delta B_{w\perp}$ for Subp #2 at $h/(V_{Aeo}/\Omega_{eo}) = -242.24$, and the corresponding energy transfers (b) ΔW_L and (c) ΔW_c . The ΔW_L is positive during subpacket formation, indicating that Landau resonant particles cause wave damping. While cyclotron resonant particles transfer energy to subpackets with a negative ΔW_c , which is consistent with Wang et al. (2024). Therefore, the wave-particle interaction through cyclotron resonance dominates the energy transfer during the formation of quasi-parallel subpackets. Note that it cannot be excluded that the interaction through Landau resonance might be dominant in the highly oblique subpackets.

In this study, we modify the theoretical trapping frequency ω_{tr_NL} by considering different inhomogeneity factor S . Moreover, we establish the relation between ω_{tr_NL} and ω_{subp} in Equation 14, facilitating the estimation of ω_{tr_NL} through directly measurement of ω_{subp} in observations of intense subpackets. This equation is also applicable to Landau resonant electrons, which move together with subpackets. Equation 14 can be simplified to $\omega_{tr_NL} \approx \omega_{subp}$, consistent with previous results (O'Neil, 1965). Note that in this scenario, ω_{subp} represents the reverse period of wave amplitude modulation.

Data Availability Statement

All the data from Van Allen Probes were from <https://spdf.gsfc.nasa.gov/pub/data/rbsp/>. The simulation data are available in H. Chen (2024).

Acknowledgments

This work was supported by the NASA Grants 80NSSC24K0174, 80NSSC21K1688, 80NSSC21K1679, 80NSSC20K1322, 80NSSC23K0086, 80NSSC22K1012, and the NSF Grants AGS-2131012, AGS-2247759, and AGS-2224109. LC and ZX were supported by the NASA Grant 80NSSC21K1320 and the NSF Grant AGS-2225121. YO and YH were supported by JSPS KAKENHI Grants JP20H01960 and JP23H05429. Computer resources are provided by NASA NAS Division.

References

- Albert, J. M., Artemyev, A. V., Li, W., Gan, L., & Ma, Q. (2021). Models of resonant wave-particle interactions. *Journal of Geophysical Research: Space Physics*, 126(6), e2021JA029216. <https://doi.org/10.1029/2021JA029216>
- Bortnik, J., Thorne, R. M., & Inan, U. S. (2008). Nonlinear interaction of energetic electrons with large amplitude chorus. *Geophysical Research Letters*, 35(21), L21102. <https://doi.org/10.1029/2008GL035500>
- Chen, H. (2024). Database of “nonlinear electron trapping through cyclotron resonance in the formation of chorus wave subpackets” [Dataset]. *Zenodo*. <https://doi.org/10.5281/zenodo.10822409>
- Chen, H., Lu, Q., Wang, X., Fan, K., Chen, R., & Gao, X. (2022). One-dimensional gcPIC- δf simulation of hooked chorus waves in the Earth’s inner magnetosphere. *Geophysical Research Letters*, 49(4), e2022GL097989. <https://doi.org/10.1029/2022GL097989>
- Chen, H., Wang, X., Chen, L., Omura, Y., Lu, Q., Chen, R., et al. (2023). Simulation of downward frequency chirping in the rising tone chorus element. *Geophysical Research Letters*, 50(9), e2023GL103160. <https://doi.org/10.1029/2023GL103160>
- Chen, H., Wang, X., Chen, L., Omura, Y., Tsurutani, B. T., Lin, Y., & Xia, Z. (2023). Evolution of chorus subpackets in the Earth’s magnetosphere. *Geophysical Research Letters*, 50(21), e2023GL105938. <https://doi.org/10.1029/2023GL105938>
- Chen, R., Tsurutani, B. T., Gao, X., Lu, Q., Chen, H., Lakhina, G. S., & Hajra, R. (2022). The structure and microstructure of rising-tone chorus with frequencies crossing at $f \sim 0.5$ fce. *Journal of Geophysical Research: Space Physics*, 127(8), e2022JA030438. <https://doi.org/10.1029/2022JA030438>
- Crabtree, C., Ganguli, G., & Tejero, M. (2017). Analytical and numerical analysis of self-consistent whistler wave Hamiltonian. *Plasma Physics and Controlled Fusion*, 59(11), 114002. <https://doi.org/10.1088/1361-6587/aa837a>
- Crabtree, C., Tejero, E., Ganguli, G., Hospodarsky, G. B., & Kletzing, C. A. (2017). Bayesian spectral analysis of chorus subelements from the Van Allen Probes. *Journal of Geophysical Research: Space Physics*, 122(6), 6088–6106. <https://doi.org/10.1002/2016JA023547>
- Demekhov, A. G., Taubenschuss, U., Hanzelka, M., & Santolík, O. (2020). Frequency dependence of very low frequency chorus pointing flux in the source region: THEMIS observations and a model. *Geophysical Research Letters*, 47(6), e2020GL086958. <https://doi.org/10.1029/2020GL086958>
- Denavit, J., & Sudan, R. N. (1975). Whistler sideband instability. *Physics of Fluids*, 18(5), 575–584. <https://doi.org/10.1063/1.861173>
- Foster, J. C., Erickson, P. J., Omura, Y., Baker, D. N., Kletzing, C. A., & Claudepierre, S. G. (2017). Van Allen Probes observations of prompt MeV radiation belt electron acceleration in nonlinear interactions with VLF chorus. *Journal of Geophysical Research: Space Physics*, 122(1), 324–339. <https://doi.org/10.1002/2016JA023429>
- Goyal, R., Sharma, R. P., & Kumar, S. (2017). Nonlinear effects associated with quasi-electrostatic whistler waves relevant to that in radiation belts. *Journal of Geophysical Research: Space Physics*, 122(1), 340–348. <https://doi.org/10.1002/2016JA023274>
- Hanzelka, M., Santolík, O., Omura, Y., Kolmašová, I., & Kletzing, C. A. (2020). A model of the subpacket structure of rising tone chorus emissions. *Journal of Geophysical Research: Space Physics*, 125(8), e2020JA028094. <https://doi.org/10.1029/2020JA028094>
- Hiraga, R., & Omura, Y. (2020). Acceleration mechanism of radiation belt electrons through interaction with multi-subpacket chorus waves. *Earth Planets and Space*, 72(1), 21. <https://doi.org/10.1186/s40623-020-1134-3>
- Kataoka, R., Miyoshi, Y., Hampton, D., Ishii, T., & Kozako, H. (2012). Pulsating aurora beyond the ultra-low-frequency range. *Journal of Geophysical Research*, 117(A8), A08336. <https://doi.org/10.1029/2012JA017987>
- Kubota, Y., & Omura, Y. (2018). Nonlinear dynamics of radiation belt electrons interacting with chorus emissions localized in longitude. *Journal of Geophysical Research: Space Physics*, 123(6), 4835–4857. <https://doi.org/10.1029/2017JA025050>
- Lu, Q., Ke, Y., Wang, X., Liu, K., Gao, X., Chen, L., & Wang, S. (2019). Two-dimensional general curvilinear particle-in-cell (gcPIC) simulation of rising-tone chorus waves in a dipole magnetic field. *Journal of Geophysical Research: Space Physics*, 124(6), 4157–4167. <https://doi.org/10.1029/2019JA026586>
- Menietti, J. D., Shprits, Y. Y., Horne, R. B., Woodfield, E. E., Hospodarsky, G. B., & Gurnett, D. A. (2012). Chorus, ECH, and Z mode emissions observed at Jupiter and Saturn and possible electron acceleration. *Journal of Geophysical Research*, 117(A12), A12214. <https://doi.org/10.1029/2012JA018187>
- Miyoshi, Y., Saito, S., Seki, K., Nishiyama, T., Kataoka, R., Asamura, K., et al. (2015). Relation between fine structure of energy spectra for pulsating aurora electrons and frequency spectra of whistler mode chorus waves. *Journal of Geophysical Research: Space Physics*, 120(9), 7728–7736. <https://doi.org/10.1002/2015JA021562>
- Mourenas, D., Zhang, X.-J., Nunn, D., Artemyev, A. V., Angelopoulos, V., Tsai, E., & Wilkins, C. (2022). Short chorus wave packets: Generation within chorus elements, statistics, and consequences on energetic electron precipitation. *Journal of Geophysical Research: Space Physics*, 127(5), e2022JA030310. <https://doi.org/10.1029/2022JA030310>
- Nogi, T., & Omura, Y. (2022). Nonlinear signatures of VLF-triggered emissions: A simulation study. *Journal of Geophysical Research: Space Physics*, 127(1), e2021JA029826. <https://doi.org/10.1029/2021JA029826>
- Nunn, D. (1974). A self-consistent theory of triggered VLF emissions. *Planetary and Space Science*, 22(3), 349–378. [https://doi.org/10.1016/0032-0633\(74\)90070-1](https://doi.org/10.1016/0032-0633(74)90070-1)
- Nunn, D. (1986). A nonlinear theory of sideband stability in ducted whistler mode waves. *Planetary and Space Science*, 34(5), 429–451. [https://doi.org/10.1016/0032-0633\(86\)90032-2](https://doi.org/10.1016/0032-0633(86)90032-2)
- Nunn, D., Zhang, X.-J., Mourenas, D., & Artemyev, A. V. (2021). Generation of realistic short chorus wave packets. *Geophysical Research Letters*, 48(7), e2020GL092178. <https://doi.org/10.1029/2020GL092178>
- Omura, Y. (2021). Nonlinear wave growth theory of whistler-mode chorus and hiss emissions in the magnetosphere. *Earth Planets and Space*, 73(1), 1–28. <https://doi.org/10.1186/s40623-021-01380-w>
- Omura, Y., Katoh, Y., & Summers, D. (2008). Theory and simulation of the generation of whistler-mode chorus. *Journal of Geophysical Research*, 113(A4), A04223. <https://doi.org/10.1029/2007JA012622>
- O’Neil, T. (1965). Collisionless damping of nonlinear plasma oscillations. *Physics of Fluids*, 8(12), 2255–2262. <https://doi.org/10.1063/1.1761193>
- Ozaki, M., Shiokawa, K., Miyoshi, Y., Hosokawa, K., Oyama, S., Yagitani, S., et al. (2018). Microscopic observations of pulsating aurora associated with chorus element structures: Coordinated Arase satellite-PWING observations. *Geophysical Research Letters*, 45(22), 12125–12134. <https://doi.org/10.1029/2018GL079812>
- Reinlein, L. A., Kurth, W. S., & Gurnett, D. A. (1984). Chorus-related electrostatic bursts at Jupiter and Saturn. *Journal of Geophysical Research*, 89(A1), 75–83. <https://doi.org/10.1029/JA089i001p00075>
- Santolík, O., Gurnett, D. A., Pickett, J. S., Parrot, M., & Cornilleau-Wehrlin, N. (2003). Spatio-temporal structure of storm-time chorus. *Journal of Geophysical Research*, 108(A7), 1278. <https://doi.org/10.1029/2002JA009791>

- Sudan, R. N., & Ott, E. (1971). Theory of triggered VLF emissions. *Journal of Geophysical Research*, 76(19), 4463–4476. <https://doi.org/10.1029/JA076i019p04463>
- Tao, X., Zonca, F., & Chen, L. (2017). Identify the nonlinear wave-particle interaction regime in rising tone chorus generation. *Geophysical Research Letters*, 44(8), 3441–3446. <https://doi.org/10.1002/2017GL072624>
- Tao, X., Zonca, F., & Chen, L. (2021). A “Trap-Release-Amplify” model of chorus waves. *Journal of Geophysical Research: Space Physics*, 126(9), e2021JA029585. <https://doi.org/10.1029/2021JA029585>
- Tsurutani, B. T., Chen, R., Gao, X., Lu, Q., Pickett, J. S., Lakhina, G. S., et al. (2020). Lower-band “monochromatic” chorus riser subelement/wave packet observations. *Journal of Geophysical Research: Space Physics*, 125(10), e2020JA028090. <https://doi.org/10.1029/2020JA028090>
- Tsurutani, B. T., Verkhoglyadova, O. P., Lakhina, G. S., & Yagitani, S. (2009). Properties of dayside outer zone chorus during HILDCAA events: Loss of energetic electrons. *Journal of Geophysical Research*, 114(A3), A03207. <https://doi.org/10.1029/2008JA013353>
- Van Compernolle, B., An, X., Bortnik, J., Thorne, R. M., Pribyl, P., & Gekelman, W. (2016). Excitation of chirping whistler waves in a laboratory plasma. *Physical Review Letters*, 114(24), 245002. <https://doi.org/10.1103/PhysRevLett.114.245002>
- Wang, X., Chen, H., Omura, Y., Hsieh, Y.-K., Chen, L., Lin, Y., et al. (2024). Resonant electron signatures in the formation of chorus wave subpackets. *Geophysical Research Letters*, 51(8), e2023GL108000. <https://doi.org/10.1029/2023GL108000>
- Zhang, X.-J., Mourenas, D., Artemyev, A. V., Angelopoulos, V., Kurth, W. S., Kletzing, C. A., & Hospodarsky, G. B. (2020). Rapid frequency variations within intense chorus wave packets. *Geophysical Research Letters*, 47(15), e2020GL088853. <https://doi.org/10.1029/2020GL088853>
- Zhang, X.-J., Thorne, R., Artemyev, A., Mourenas, D., Angelopoulos, V., Bortnik, J., et al. (2018). Properties of intense field-aligned lower-band chorus waves: Implications for nonlinear wave-particle interactions. *Journal of Geophysical Research: Space Physics*, 123(7), 5379–5393. <https://doi.org/10.1029/2018JA025390>
- Zonca, F., Tao, X., & Chen, L. (2022). A theoretical framework of chorus wave excitation. *Journal of Geophysical Research: Space Physics*, 127(2), e2021JA029760. <https://doi.org/10.1029/2021JA029760>

References From the Supporting Information

- Hsieh, Y.-K., & Omura, Y. (2023). Precipitation rates of electrons interacting with lower-band chorus emissions in the inner magnetosphere. *Journal of Geophysical Research: Space Physics*, 128(6), e2023JA031307. <https://doi.org/10.1029/2023JA031307>